Soft Matter

PAPER

From macro- to microscale poroelastic characterization of polymeric hydrogels *via* indentation†

Z. Ilke Kalcioglu,‡[a] Roza Mahmoodian,‡[a] Yuhang Hu,[b] Zhigang Suo[b] and Krystyn J. Van Vliet*[ac]

Recent advances in contact mechanics have formalized approaches to distinguish between poroelastic and viscoelastic deformation regimes *via* load relaxation experiments, and to simultaneously extract the mechanical and transport properties of gels at the macroscale. As poroelastic relaxation times scale quadratically with contact diameter, contact radii and depths on the mm scale can require hours for a single load relaxation experiment to complete. For degradable materials such as biodegradable hydrogels and soft biological tissues, it is necessary to minimize the required experimental time. Here, we investigated the applicability of these methods at smaller (μm) length scales to shorten relaxation times. We conducted load relaxation experiments on hydrated polyacrylamide (PAAm) gels at the microscale *via* atomic force microscopy (AFM)-enabled indentation, as well as at the macroscale *via* instrumented indentation. We confirmed the approach as a reliable means to distinguish between viscoelastic and poroelastic relaxation regimes at the microscale: shear modulus G, drained Poisson's ratio ν_s, diffusivity D, and intrinsic permeability κ of the gels agreed well at the micro- and macroscale levels. Importantly, these properties were accessed accurately within seconds at the microscale, rather than within hours at the macroscale. Our results demonstrate the promise of contact-based load relaxation analysis toward rapid, robust characterization of mechanical and transport properties for poroelastic gels and tissues.

1. Introduction

Instrumented indentation is a well-established approach to measure mechanical properties of materials. Initially utilized to characterize elastic and plastic properties of metals and ceramics,[1] such experiments have been applied more recently to characterize viscoelastic and poroelastic regimes in relatively more compliant materials including polymeric gels and so-called biological soft tissues.[2–10]

Polymeric gels, consisting of a network of cross-linked polymer chains swollen with a solvent, are a class of gels with widespread application in which the solid network deformation and solvent flow are coupled. Scherer[11,12] provided the analytical foundation[13,14] and a novel test[13] to obtain elastic and viscoelastic properties and permeability of aerogel beams during bending. However, this beam-bending approach is difficult to implement

for increasingly compliant materials (Young's elastic modulus $E < 1$ MPa). Hui *et al.* recently presented a contact-based theoretical approach to extract simultaneously the mechanical and transport properties of hydrated gels *via* cylindrical punch indentation,[14] whereby the load relaxation response was related to the shear modulus, Poisson's ratio, diffusivity, and intrinsic permeability of a gel. To extend this load relaxation approach to other indenter geometries, Lin *et al.* and Hu *et al.* utilized finite element analyses to obtain semi-analytical relations between the initial and fully relaxed load for a flat rigid circular punch,[15] rigid rectangular punch,[16] and conical and spherical punches.[17,18]

One important characteristic of gels and other fluid-filled materials is that the mechanical response can depend on both the time scale and length scale of measurements. Since the time dependence of a linear viscoelastic response is independent of the contact diameter, whereas the poroelastic response is dependent on the contact diameter, the aforementioned approaches provide a means to distinguish between load relaxation resulting from viscoelastic relaxation of the gel network and that resulting from solvent flow. In fact, Hu *et al.*[17,18] adopted a facile scaling means to identify dominance of the poroelastic deformation regime, so that experiments could be designed to extract both the elastic and transport properties of gels. To date, however, these methods have been applied only at the macroscale level for probe diameters on the order of cm. Since the poroelastic relaxation time

[a] Department of Materials Science and Engineering, Massachusetts Institute of Technology, 77 Massachusetts Avenue, Cambridge, MA 02139, USA. E-mail: krystyn@mit.edu
[b] School of Engineering and Applied Sciences, Kavli Institute, Harvard University, Cambridge, MA 02138, USA
[c] Department of Biological Engineering, Massachusetts Institute of Technology, 77 Massachusetts Avenue, Cambridge, MA 02139, USA
† Electronic supplementary information (ESI) available. See DOI: 10.1039/c2sm06825g
‡ These authors contributed equally.

τ scales quadratically with contact diameter, relaxation times in such experiments are on the order of hours. This length–time scale coupling renders experiments quite time consuming, which constrains the range of material systems that can be studied. In particular, it is not feasible to analyze the poroelastic response of soft biological tissues or degradable gels that require mechanical analysis under hydrated conditions over durations that are longer than the degradation time scales that naturally affect the structure and properties. Further, macroscale analysis of poroelastic properties restricts treatment of materials such as striated tissues that exhibit structural transitions at smaller (*e.g.*, μm) length scales.

Here, we sought to extend and validate the load relaxation approach of Hu *et al.* to smaller length and time scales, which would enable future studies on degrading or structurally heterogeneous gels and tissues. We compared analysis at the micro- and macroscale levels for a polyacrylamide (PAAm) hydrogel to determine whether poroelasticity could be identified as the dominant regime at the microscale, and to determine whether the elastic and transport properties could be extracted accurately and more rapidly than is possible at the macroscale.

2. Materials and methods

2.1 Materials

Acrylamide stock solution was prepared by mixing 40% w/v acrylamide, 2% bis-acrylamide solution (Bio-Rad) and distilled water in a ratio of 1 : 2 : 2. After degassing the solution for 20 min, gels were synthesized by adding initiators of 10% w/v ammonium persulfate solution and N,N,N',N'-tetramethylethylenediamine (TEMED) to the stock solution. For macroscale experiments, three different gels were cast into 60 mm diameter polystyrene Petri dishes to form a hydrated thickness of 1 cm. For microscale experiments, three different gels from the same batch synthesis were cast onto silane-treated glass slides. Prior to casting, glass slides were treated with 5 vol% glutaraldehyde, which was then aspirated and rinsed, to ensure that the gels adhered well to the glass substrate. Gels measured 22 mm × 22 mm in-plane with a hydrated thickness of 500 μm. After 30 min gelation at room temperature, gels were submerged in phosphate buffered solution (DPBS, Invitrogen) and were maintained fully hydrated at 4 °C for two weeks prior to testing to attain swelling equilibrium.

2.2 Macroscale load relaxation experiments

Macroscale load relaxation experiments were conducted using a custom-built load frame with a force resolution of 50 μN and a displacement resolution of 1 μm, as described previously.[17] Experiments were conducted *via* a stainless steel spherical probe of 1 cm radius (Fig. 1a). The instrument was programmed to approach the surface of PAAm gels at a rate of 2 μm s^{-1}, until a positive slope of the force–displacement response was recorded. Upon contact detection, indenter displacement was increased with a rise time of 2 s to attain three maximum indentation depths, h_{max} = 100, 200, or 400 μm. For each maintained depth, load relaxation measurements were acquired in triplicate over approximately 20, 40, and 110 h, respectively. Gels were fully submerged in DPBS solution in all experiments.

2.3 Microscale load relaxation experiments

Microscale load relaxation experiments were conducted using atomic force microscopy (AFM)-enabled indentation (3D Molecular Force Probe, Asylum Research, Santa Barbara, CA) (Fig. 1b). Spherical polystyrene cantilevers (Novascan) with a nominal probe radius of 22.5 μm and spring constant k of 14.0 N m^{-1} were used; actual values of k were determined experimentally for each cantilever.[7] Upon automatic contact detection (based on cantilever deflection), indenter displacement was increased at a velocity of 50 μm s^{-1} to attain three maximum depths, h_{max} = 4, 6 and 8 μm. For each maintained depth, 45 replicate load relaxation experiments were acquired over 20–30 s, with a sampling rate of 250 Hz to acquire sufficient data for accurate analysis. To examine repeatability and potential structural heterogeneities at this lower length scale, n = 45 replicate measurements at each depth were attained by acquiring five replicate measurements (within an area of 80 μm × 80 μm) at three different locations on each of the three samples.

2.4 Analysis

We adapted the method of Hu *et al.*[17,18] to analyze the acquired load relaxation responses. We summarize here the necessary equations to identify the dominance of the poroelastic deformation regime and the extraction of elastic and transport properties.

After an indenter is pressed into a gel to a fixed depth h, the force on the indenter relaxes as a function of time $F(t)$. At sufficiently short times, the gel behaves as an incompressible material because there is no time for fluid to leave the network, while at extended times it acts as a compressible material. For a spherical indenter pressed into an incompressible elastic solid, the force on the indenter is given by:[19]

$$F_0 = 16/3 Gah \quad (1)$$

where F_0 is the resulting force at $t = 0$, G is the shear modulus, and a is the radius of contact computed from $a = \sqrt{Rh}$. The ratio of the initial force F_0 and fully relaxed force at long times F_∞ is related to the Poisson's ratio of the solid v_s as:

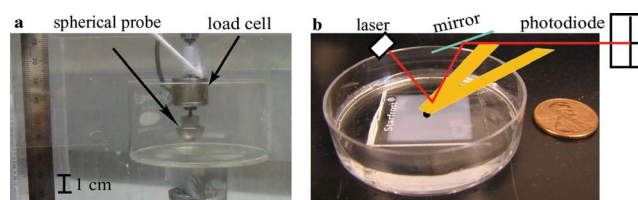$$\frac{F_0}{F_\infty} = 2(1 - v_s) \quad (2)$$

Fig. 1 (a) Apparatus for load relaxation experiments at the macroscale, using a stainless steel spherical probe of radius 1 cm. Scale marker at left is in cm. (b) Schematic of the load relaxation experiment conducted at the microscale, using a polystyrene spherical probe of radius 22.5 μm attached to the cantilever of an atomic force microscope. All experiments were conducted on fully hydrated polyacrylamide gels immersed in buffered saline solution.

From the experimental data, G and ν_s can be readily determined using eqn (1) and (2). Since the relevant length scale in this problem is the radius of contact a, the normalized time takes the form t/τ where $\tau = D/a^2$ is the characteristic relaxation time constant, and the force $F(t)$ is given for a spherical indenter as:

$$\frac{F(t) - F_\infty}{F_0 - F_\infty} = 0.491\exp\left(-0.908\sqrt{\tau}\right) + 0.509\exp\left(-1.679\tau\right) \quad (3)$$

where the magnitudes of prefactors were obtained by Hu et al. from finite element simulations.[17] In the present analysis, the dominant mechanism of load relaxation was determined by normalizing the force according to eqn (3) and the time by a^2. The relaxation time of a material that behaves linear viscoelastically is independent of the contact diameter, whereas the poroelastic relaxation time is length scale dependent. Therefore, by normalizing time by the relevant length scale (a^2), it is possible to differentiate between these two regimes. In other words, if after normalizing time by a^2, the normalized force–time responses collapse, it is inferred that poroelastic relaxation was dominant. The opposite is concluded if little or no length scale dependence is observed. To render this distinction, we conducted the following analysis for both the macroscale and microscale experiments: first, we averaged the replicate load-relaxation responses at each maximum indentation depth ($n = 3$ indentation depths). This resulted in three output curves for data with only force being normalized (Fig. 3a and d), and three output curves for data with both force and time being normalized (Fig. 3b and e). Next, for a clearer manifestation of this distinction, for each type of normalization, we calculated the standard deviation among all of the replicate load-relaxation responses from the three indentation depths tested (Fig. 3c and f). Note that the standard deviation among these responses is defined here to reflect a measure of dispersion among relaxation responses measured for distinct maximum depths, while still including the experimental variation among responses at a given maximum depth. This approach serves as a means to quantify the effect of time normalization on the collapse of the response curves. For each time point, these standard deviations were calculated as:

$$s = \left(\frac{1}{n}\sum_{i=1}^{n}(y_i - \bar{y})^2\right)^{\frac{1}{2}} \quad (4)$$

where $n = 9$ for macroscale and $n = 135$ for microscale experiments (corresponding to all the replicate responses from all the indentation depths tested), y_i represents the normalized force value at that particular time point for a particular output curve, and $\bar{y}$ is the average of all the normalized force values at that time point. Smaller standard deviation for a specific normalization scheme was interpreted as stronger collapse, allowing identification of the dominant regime. Previously, other forms of force normalization were used to assist in this classification.[17,18] Our rationale for departure from those approaches is addressed in the Discussion section.

Since F_0, F_∞ and $F(t)$ are known from the experiment, the only unknown parameter in eqn (3) is diffusivity D. To extract D, a custom-written optimization algorithm was used in MATLAB (The MathWorks, Natick, MA) to find the best fit of eqn (3) to the experimental force–time response. Intrinsic permeability κ is then calculated from

$$\kappa = \frac{D(1 - 2\nu_s)\eta}{2(1 - \nu_s)G} \quad (5)$$

where η is the solvent viscosity which is assumed to be equal to that of water (0.89×10^{-3} Pa s) for PAAm gels.[20] The characteristic relaxation times for the micro- and macroscale experiments are listed in Table 1. Unpaired t-tests were utilized to detect statistically significant differences among the values obtained at different maximum indentation depths (GraphPad Software, Inc., La Jolla, CA).

3. Results

Figure 2 shows the experimentally measured load relaxation response obtained for PAAm gels at the macroscale (Fig. 2a) and the microscale (Fig. 2b), indicated as the average among replicate experiments at each maximum depth. It is observed from these graphs that the time required for full relaxation exceeded tens of hours for macroscale experiments (up to 110 h), as compared to a few seconds for microscale experiments. Macroscale contact radii (1.0–2.0 mm) were three orders of magnitude larger than those in microscale experiments (9.5–13.4 μm).

The length scale dependence of relaxation time is a clear manifestation of the poroelastic response. In contrast, linear viscoelastic relaxation is independent of the contact diameter. Therefore, by normalizing time by the relevant length scale (a^2), it is possible to differentiate between the poroelastic and linear viscoelastic regimes. This point is illustrated in Fig. 3, in which load is normalized according to eqn (3). At both the micro- and macroscale, normalization of the time by a^2 resulted qualitatively in the collapse of these responses onto a single curve (Fig. 3b and e), and quantitatively to a lower standard deviation among the curves acquired at three different maximum depths (Fig. 3c and f). This qualitative and quantitative assessment of the load relaxation responses confirms that the poroelastic response is dominant for these gels at both the macro- and microscales.

Mechanical and diffusive properties are reported in Table 1, calculated according to eqn (1)–(3) and (5). The excellent agreement in all calculated properties (less than 20% difference) for experiments that analyzed the same gel over 10s of hours (with cm scale probes) and <10s of seconds (with μm scale probes) validates the application of load relaxation analysis at the microscale. Note that the characteristic poroelastic time τ is not constant for a given material (i.e., for a given gel or tissue) but rather depends strongly on the deformation length scale defined by the experiment; here, τ varied over five orders of magnitude for the range of contact radii a that varied over three orders of magnitude.

4. Discussion

In the present study we assessed the applicability of the method of Hui et al.,[14] as extended by Hu et al.,[17,18] to the study of μm scale experiments. Within the context of this theory, contact based measurements of stress relaxation provide a simpler means to determine the permeability and compressibility of gels, which would otherwise have to be obtained from independent measurements of shear modulus, longitudinal elastic modulus,[21,22] and diffusivity.[23] By appropriately analyzing stress

Table 1 Calculated shear modulus G, Poisson's ratio ν_s, diffusivity D, intrinsic permeability κ and characteristic relaxation time as a function of indentation depth for two probes of radii R_1 and R_2. Data are presented as mean ± standard deviation.

| Indentation depth	Shear modulus G/kPa	Poisson's ratio ν_s	Diffusivity D/10^{-10} m^2 s^{-1}	Intrinsic permeability κ/10^{-18} m^2	τ/s
400 μm ($R_1 = 1$ cm)	6.78 ± 0.20	0.39 ± 0.020	1.80 ± 0.25	4.78 ± 0.16	22.2 × 10^3
200 μm ($R_1 = 1$ cm)	6.70 ± 0.01	0.40 ± 0.007	1.97 ± 0.12	4.93 ± 0.86	10.2 × 10^3
100 μm ($R_1 = 1$ cm)	6.60 ± 0.10	0.41 ± 0.010	2.03 ± 0.00	5.82 ± 0.17	4.9 × 10^3
8 μm ($R_2 = 22.5$ μm)	6.21 ± 0.10	0.39 ± 0.004	1.70 ± 0.25	4.24 ± 0.51	1.06
6 μm ($R_2 = 22.5$ μm)	6.53 ± 0.13	0.38 ± 0.005	1.67 ± 0.26	4.35 ± 0.60	0.81
4 μm ($R_2 = 22.5$ μm)	6.73 ± 0.19	0.37 ± 0.005	1.60 ± 0.15	4.31 ± 0.31	0.56
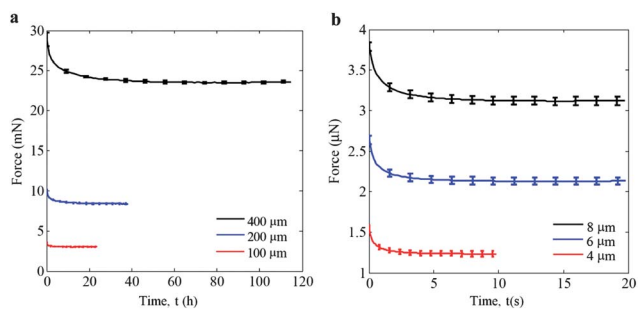
Fig. 2 (a) Load vs. time response for macroscale experiments ($R = 1$ cm) at three different maximum indentation depths (100, 200, and 400 μm), where relaxation times exceed 10s of hours. (b) Load vs. time response for microscale experiments ($R = 22.5$ μm) at three different maximum indentation depths (4, 6, and 8 μm), where relaxation times are on the order of a few seconds. Data are shown as mean ± standard deviation among replicate experiments. Due to the high data density (see text), error bars are not displayed for all data points.

relaxation experiments at the microscale using the above approach, the time required for experiments is greatly reduced, providing for convenient and reliable characterization of swollen gels and other classes of fluid-filled porous materials.

When an indenter is pressed into a gel, the load decays (relaxes) in a time-dependent manner. There are two distinct mechanisms of relaxation: viscoelastic relaxation as exhibited by dry elastomers, due to conformational changes of the polymer chains, and the fluid-induced (poroelastic) relaxation; a combination of both relaxation mechanisms is also possible as seen in soft tissues and elastomers swollen with solvent. Pavesi et al. have reported a viscoelastic relaxation time of ~3 ms for polyacrylamide chains as measured by pulsed NMR spectrometry at a frequency of 38 MHz,[24] which is at least two orders of magnitude smaller than the poroelastic relaxation times reported here; Weiss and Silberg reported viscoelastic time scales of ~0.09 to 0.16 s for polyacrylamide gels of similar concentrations.[26] While the relaxation times of a homogeneous material
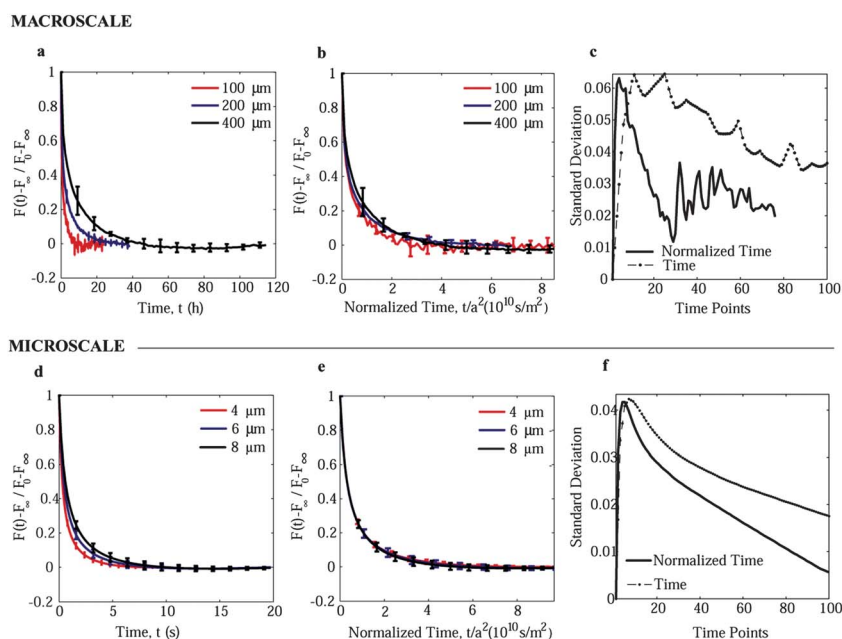

Fig. 3 Macroscale and microscale load relaxation responses for polyacrylamide gels, for which load is normalized in the form $[F(t) - F(\infty)]/[F_o - F(\infty)]$. Data are shown as mean ± standard deviation. Due to the high data density (see text), error bars are not displayed for all data points. These data do not fully collapse onto a single curve when time is not also normalized, at either the macroscale (a) or the microscale (d), as would be expected for a linear viscoelastic response. These data collapse more completely onto a single curve when time is normalized by a^2, as would be expected for a poroelastic response (b,e). Comparison of this collapse is shown in (c) and (f), as the standard deviation among the replicate curves for all maximum depths. Standard deviation is noticeably smaller when time is normalized, confirming dominance of the poroelastic regime at the macro- and microscales.

that behaves linear viscoelastically do not depend on length scales,[18] the characteristic poroelastic relaxation time of an indentation experiment is of the order of a^2/D.[14] Normalization by appropriate length scales can thus provide physical insight to distinguish between dominance of these two regimes, which is particularly advantageous when these relaxation times are of similar order. In the present study, we designed experiments that accessed poroelastic relaxation as the dominant mechanism in the PAAm gels. This is in agreement with the findings of Galli et al.,[10] who showed better matching of microindentation ($R = 400$ μm) load relaxation responses obtained for similar PAAm gels via finite element simulations assuming a poroelastic constitutive model as compared to a viscoelastic constitutive model. If the material behaved linear viscoelastically, one would expect to observe no differences in the normalized force decay as a function of different maximum indentation depths. However, Fig. 3a and d show that this is not the case for the present PAAm gels, at either the macroscale or the microscale. When additionally normalizing time by a^2, it becomes apparent in Fig. 3b and e that collapse of the responses onto a single curve is attained. This point is further underscored by the collapse of all of the normalized responses acquired at both the macroscale and microscale in a single graph (Fig. S1†), spanning four orders of magnitude in contact areas (μm^2 to mm^2). Quantitative comparisons of this strength of collapse are enabled by calculation of the standard deviation among the normalized responses, at both the macroscale and microscale (Fig. 3c and f).

Here, note that we have normalized force according to eqn (3). We wish to contrast this approach to other approaches that normalize instantaneous force by ah or by the initial force F_0.[14,17,18] This form of force normalization has been presented previously without comment;[17] here, we recognize and discuss the advantage of this choice over other approaches. The normalization of force as shown in Fig. 3 makes no a priori assumptions about how G or ν_s of the material may vary as a function of indentation depth. In contrast, normalization by ah assumes that both G and ν_s are invariant with depth into a sample, and normalization by F_0 assumes that ν_s is invariant with depth. Fig. S2† demonstrates the misinterpretations that can result by normalizing force by ah, using our data on PAAm gels as an example: at the macroscale, a poroelastic-dominant response is inferred due to the stronger collapse for time expressed as t/a^2 (Fig. S2a–c†), and at the microscale normalization by ah gives inconclusive results regarding the poroelastic dominance of load relaxation (Figs. S2d–f†). That approach assumes G and ν_s are exactly constant with indentation depth, which we showed in Table 1 is not the case for the microscale experiments; statistical analysis indicated significant differences ($p < 0.0001$) among the means of both G and ν_s obtained at the three different indentation depths. Galli et al. also noted, via comparison of experiments with finite element simulations, that G and ν_s were not identically constant with depth in similar hydrogels.[10] These differences could arise from experimental errors at small length scales due to underestimating the contact area or surface interactions between the probe and the sample.[25] However, even when such differences are statistically significant but small (<10% variation in G here among the three microscale indentation depths), this can directly affect conclusions drawn about poroelastic dominance. For example, that normalization

approach falsely indicates that the poroelastic and viscoelastic relaxation times are similar—and that poroelastic relaxation mechanisms are not dominant—under microscale deformation of these hydrogels. Similarly, Fig. S3† shows that normalization by F_0 also gives inconclusive results regarding the poroelastic dominance of load relaxation, due to the assumption of constant ν_s. Thus, although we adopt a continuum framework which assumes implicitly that the mechanical and transport properties within the deformed material volume are homogeneous, we advocate the present approach of force normalization that refrains from making any implicit assumption regarding the magnitude of mechanical properties over greater length scales.

Although there is a wide variation in levels of reported detail for polyacrylamide hydrogels (e.g., %crosslinker, %initiator, and vol% water at reaction initiation), we obtained properties that were in good agreement with those previously reported. For similarly prepared PAAm gels, Weiss et al.[26] reported elastic properties measured via force torsion pendulum-based viscoelastometry to obtain $G' = 0.3$–6 kPa; those authors separately measured transport properties in the same gels via fluid shear flow to obtain $\kappa = 7 \times 10^{-18}$ to 1.1×10^{-15} m^2. This agrees well with our finding of $G \sim 7$ kPa and $\kappa \sim 4 \times 10^{-18}$ m^2 via a single experimental approach (Table 1). Weiss et al. concluded that the network became less permeable as the gel concentration and crosslinking density increased. Since storage moduli are also related directly to gel concentration and crosslinking density,[27] this trend can explain the difference among permeability measured for different PAAm hydrogels. For example, Galli et al.[10] measured lower permeability ($\kappa = 5.6 \times 10^{-20}$ to 1.2×10^{-19} m^2) for much stiffer PAAm gels ($G \sim 100$ kPa) than those considered here. With the present method, we also found internally consistent results between the properties obtained for identically prepared samples that were examined at the microscale over (O)10 seconds and at the macroscale over (O)10s of hours; see Table 1. Thus, this approach can now be extended reliably to the microscale, with markedly decreased experimental time.

Note that although the elastic and transport properties are defined by the solid and fluid compositions of the hydrogel itself, the measured poroelastic relaxation time is also a function of the experimental length scales. This natural variation of τ with length and the requirement that sufficient relaxation occurs to enable fitting of the relaxation response to obtain poroelastic properties give rise to important considerations of experimental design at the microscale. The key to achieving reliable results with this approach is ensuring that the poroelastic relaxation time extends well beyond the rise time t_r (i.e., the time required for the instrument to reach the maximum indentation depth, after which measurement of load relaxation commences). We found that calculated relaxation times (here, 0.6 to 1 s) should be at least an order of magnitude larger than the shortest achievable rise times (for our instrument, 0.08–0.16 s) to capture sufficient relaxation required for robust fits to eqn (3) and thus robust property calculations. Generally, this minimum rise time corresponds to the maximum achievable displacement rates of a particular instrument, since true step displacements or step loads are not possible in practice. Thus, given t_r we can estimate a lower-bound value for τ to capture material relaxation response. Since τ is a function of both diffusivity and contact area as $\tau \approx a^2/D$, one

can estimate the contact areas required to maximize poroelastic relaxation times for a given material by assuming an initial estimate of diffusivity D. For the AFM-enabled load relaxation experiments conducted herein, the largest available contact areas and the shortest rise times (fastest displacement rates) were chosen to maximize the calculated relaxation time τ and to minimize relaxation during the initial displacement to attain h_{max}, respectively. To maximize the contact areas, we selected the largest AFM-cantilevered probe radius commercially available ($R = 22.5 \mu m$) and a stiff cantilever ($k_c = 14 \text{ N m}^{-1}$); the latter consideration increased the maximum accessible forces, and hence the maximum indentation depths, to result in larger contact areas and consequently in longer relaxation times. For materials of greater fluid permeability than those considered here, the contact depths and/or probe diameter must be increased in order to capture the poroelastic relaxation response.

In conclusion, we have demonstrated that the mechanical and transport properties of poroelastic materials can be measured *via* microscale load relaxation. This extension of macroscale analysis was enabled by designing experiments that accessed the poroelastic regime and identified this regime as the dominant relaxation mechanism without making *a priori* assumptions regarding the properties of the material. As there exist no analytical solutions to indentation of a poroelastic half-space, previous demonstration of this method at the macroscale obviated inference of such properties *via* finite element simulations or numerical implementation of the resulting boundary value problem. Our present validation of this approach for μm scale contact radii and contact depths significantly reduces the required experiment time scale from >10s of hours to <10s of seconds. This decreased duration extends the applicability of contact-based analysis of poroelasticity to a wider range of materials, including synthetic hydrogels and biological tissues that can degrade quickly with time.

Acknowledgements

References

1 W. C. Oliver and G. M. Pharr, *J. Mater. Res.*, 1992, **7**, 1564.
2 L. Pruitt and K. King, *J. Biomed. Mater. Res., Part A*, 2006, **78**, 729.
3 D. M. Ebenstein, A. Kuo, J. J. Rodrigo, A. H. Reddi, M. Ries and L. Pruitt, *J. Mater. Res.*, 2004, **19**, 273.
4 D. M. Ebenstein and L. A. Pruitt, *Nano Today*, 2006, **1**, 26.
5 J. D. Kaufman, G. J. Miller, E. F. Morgan and C. M. Klapperich, *J. Mater. Res.*, 2008, **23**, 1472.
6 G. Constantinides, I. Z. Kalcioglu, M. McFarland, J. F. Smith and K. J. Van Vliet, *J. Biomech. Eng.*, 2008, **41**, 3285.
7 *Handbook of Nanoindentation with Biological Applications*, ed. M. L. Oyen, Pan Stanford, Cambridge, 2011.
8 M. Galli and M. L. Oyen, *Comput. Model. Eng. Sci.*, 2009, **48**, 241–268.
9 M. Galli and M. L. Oyen, *Appl. Phys. Lett.*, 2008, **93**, 031911.
10 M. Galli, K. S. C. Comley, T. A. V. Shean and M. L. Oyen, *J. Mater. Res.*, 2009, **24**, 973.
11 G. W. Scherer, *J. Non-Cryst. Solids*, 1989, **109**, 171–182.
12 G. W. Scherer, *J. Non-Cryst. Solids*, 1989, **113**, 107–118.
13 G. W. Scherer, *J. Non-Cryst. Solids*, 1992, **142**, 18–35.
14 C.-Y. Hui, Y. Y. Lin, F.-C. Chuang, K. R. Schull and W.-C. Lin, *J. Polym. Sci., Part B: Polym. Phys.*, 2006, **44**, 359–370.
15 Y.-Y. Lin and B.-W. Hu, *J. Non-Cryst. Solids*, 2006, **352**, 4034–4040.
16 W.-C. Lin, K. R. Shull, C.-Y. Hui and Y.-Y. Lin, *J. Chem. Phys.*, 2007, **127**, 094906.
17 Y. Hu, X. Zhao, J. J. Vlassak and Z. Suo, *Appl. Phys. Lett.*, 2010, **96**, 121904.
18 Y. Hu, X. Chen, G. M. Whitesides, J. J. Vlassak and Z. Suo, *J. Mater. Res.*, 2011, **26**, 785.
19 I. N. Sneddon, *Int. J. Eng. Sci*, 1965, **3**, 47–57.
20 M. L. Oyen, *J. Mater. Res.*, 2008, **23**, 1307.
21 A. M. Hecht and E. Geissler, *Polymer*, 1980, **21**, 1358.
22 E. Geissler and A. M. Hecht, *Macromolecules*, 1981, **14**, 185.
23 A. M. Hecht, E. Geissler and A. Chosson, *Polymer*, 1981, **22**, 877.
24 L. Pavesi and A. Rigamonti, *Phys. Rev. E: Stat., Nonlinear, Soft Matter Phys.*, 1995, **51**, 3318–3323.
25 A. Engler, L. Bacakova, C. Newman, A. Hategan, M. Griffin and D. Discher, *Biophys. J.*, 2004, **86**, 617.
26 N. Weiss and A. Silberberg, *Br. Polym. J.*, 1977, **9**, 144–150.
27 C. A. Grattoni, H. H. Al-Sharji, C. Yang, A. H. Muggeridge and R. W. Zimmerman, *J. Colloid Interface Sci.*, 2001, **240**, 601–607.